Supplemental material to this article can be found at:
http://molpharm.aspetjournals.org/content/suppl/2021/06/28/molpharm.120.000202.DC1
1521-0111/100/3/193–202$35.00
MOLECULAR PHARMACOLOGY
https://doi.org/10.1124/molpharm.120.000202
Mol Pharmacol 100:193–202, September 2021

Selection and Characterization of FD164, a High-Affinity Signal Regulatory Protein α Variant with Balanced Safety and Effectiveness, from a Targeted Epitope Mammalian Cell-Displayed Antibody Library[S]

Zhihong Wang,[1] Naijing Hu,[1] Xinying Li,[1] Haitao Wang, Caiping Ren, Chunxia Qiao, Guojiang Chen, Jing Wang, Liuzhong Zhou, Jiaguo Wu, Dingmu Zhang, Jiannan Feng, Beifen Shen, Hui Peng, and Longlong Luo

State Key Laboratory of Toxicology and Medical Countermeasures, Beijing Institute of Pharmacology and Toxicology, Beijing, China (Z.W., N.H., X.L., C.Q., G.C., J.W., L.Z., J.W., D.Z., J.F., B.S., L.L.); School of Basic Medicine and Clinical Pharmacy, China Pharmaceutical University, Nanjing, China (H.W., H.P.); Department of Operational Medicine, Tianjin Institute of Environmental & Operational Medicine, Tianjin, China (H.P.); Department of Hematology, Fourth Medical Center, Chinese PLA General Hospital, Beijing, China (H.W.); and Cancer Research Institute, School of Basic Medical Science, Central South University, Changsha, China (C.R.)

Received November 05, 2020; accepted June 11, 2021

ABSTRACT

Phagocytic resistance plays a key role in tumor-mediated immune escape, so phagocytosis immune checkpoints are a potential target for cancer immunotherapy. CD47 is one of the important phagocytosis immune checkpoints; thus, blocking the interaction between CD47 and signal regulatory protein α (SIRPα) may provide new options for cancer treatment. Using computer-aided targeted epitope mammalian cell-displayed antibody library, we screened and obtained an engineered SIRPα variant fragment crystallizable fusion protein, FD164, with higher CD47-binding activity than wild-type SIRPα. Compared with wild-type SIRPα, FD164 has approximately 3-fold higher affinity for binding to CD47, which further enhanced its phagocytic effect in vitro and tumor suppressor activity in vivo. FD164 maintains the similar antitumor activity of the clinical research drug Hu5F9 in the mouse xenograft model. Furthermore, FD164 combined with rituximab can significantly improve the effect of single-agent therapy. On the other hand, compared with Hu5F9, FD164 does not cause hemagglutination, and its ability to bind to red blood cells or white blood cells is weaker at the same concentration. Finally, it was confirmed by computer structure prediction and alanine scanning experiments that the N^{45}, E^{47}, ^{52}TEVYVK^{58}, K^{60}, ^{115}EVTELTRE^{122}, and E^{124} residues of CD47 are important for SIRPα or FD164 recognition. Briefly, we obtained a high-affinity SIRPα variant FD164 with balanced safety and effectiveness.

SIGNIFICANCE STATEMENT

Up to now, few clinically marketed drugs targeting CD47 have been determined to be effective and safe. FD164, a potential signal regulatory protein α variant fragment crystallizable protein with balanced safety and effectiveness, could provide a reference for the development of antitumor drugs.

Introduction

Cancer immunotherapy has become an increasingly successful strategy in recent years. It has spawned immune checkpoint inhibitors (such as nivolumab or ipilimumab) (Darvin et al., 2018), cell adoptive immunotherapy represented by chimeric antigen receptor T-cell therapy (Labanieh et al., 2018; Wang et al., 2017), and cancer vaccines based on tumor-specific antigens or tumor-associated antigens (Banchereau and Palucka, 2018). This field has completely subverted the traditional tumor diagnosis and treatment model and brings great hope to some patients with refractory advanced tumors. In targeted acquired immunity, T-cell immune checkpoints, such as cytotoxic T-lymphocyte–associated antigen-4 and programmed cell death protein 1, have been considered a major breakthrough in clinical practice. However, cancer immunotherapy also faces the dilemma of a low response rate and a high incidence of side effects (Eggermont et al., 2016; Eggermont et al., 2015; Ribas et al., 2016). In addition, due to individual differences in patients, primary or acquired resistance occurs in immunotherapy during clinical treatment (O'Donnell et al., 2017; Sharma et al., 2017). Many clinical and related studies have found that the

The work was supported by grants from the National Natural Sciences Foundation of China [No. 31771010, No. 81700122, No. 81773755].
[1]These authors contributed equally.
dx.doi.org/10.1124/molpharm.120.000202.
[S] This article has supplemental material available at mol.aspetjournals.org.

ABBREVIATIONS: APC, allophycocyanin; CFSE, carboxyfluorescein succinimidyl ester; CVFF, consistent valence force field; Fc, fragment crystallizable; M-CSF, macrophage colony stimulating factor; OD, optical density; PCR, polymerase chain reaction; PDB, Protein Data Bank; PE, phycoerythrin; SIRPα, signal regulatory protein α; TGI, tumor growth inhibition value; V1, variant 1.

new immune checkpoint mechanisms and combination therapies can solve the current situation of the low response rate of anti–programmed cell death protein 1 or anti–programmed cell death ligand 1 monotherapy to a certain extent.

Innate immunity system not only is the body's first line of defense against external pathogenic microorganisms but also is responsible for monitoring and eliminating tumor cells. However, tumor cells can also induce specific mechanisms to avoid the recognition by the innate immune system, thereby achieving "tumor immune escape" (Chao et al., 2011). Even in certain cases, tumor cells trick tumor-infiltrating immune cells into a tumor-promoting state (Belgiovine et al., 2016; Qian and Pollard, 2010; Zabuawala et al., 2010). CD47 is an important innate immunity checkpoint that acts as a receptor for signal regulatory protein α (SIRPα) and transmits a signal of "don't eat me" (Koh et al., 2017; Matlung et al., 2017; Veillette and Chen, 2018), which may affect the proliferation, migration, and invasion of tumor cells and cause obstacles to immune cell proliferation and eventually apoptosis (Barclay and Brown, 2006). Most notably, CD47 is highly expressed on almost all tumor cells, such as non-Hodgkin lymphoma, acute myeloid leukemia, gastric cancer, lung cancer, liver cancer, and breast cancer (Barrera et al., 2017; Galli et al., 2015; Starr et al., 2013; Sudo et al., 2017), and these malignant tumor cells escape phagocytosis and killing through the CD47/SIRPα signaling axis. Previous studies have confirmed that blocking the CD47-SIRPα interaction can effectively inhibit tumor progression (Kaur et al., 2016; Liu et al., 2015; Ma et al., 2020; Petrova et al., 2017; Weiskopf et al., 2016; Xiao et al., 2015). Therefore, antibodies or fusion protein drugs targeting the CD47/SIRPα signaling axis are expected to become highly effective clinical cancer therapies (Kauder et al., 2018; Petrova et al., 2017; Veillette and Chen, 2018).

To date, more than 20 antibody drugs targeting CD47 or SIRPα have undergone preclinical evaluation or clinical trials, most of which are in phase I clinical trials, but they still face the challenge of hematologic toxicity. For example, Hu5F9, a drug in phase II clinical trials, causes erythrocyte agglutination and hemolysis (Sikic et al., 2019; Velliquette et al., 2019). Given the clinical advantages of targeting CD47, more differentiated drug designs, screening methods, and clinical development strategies are needed to obtain much safer and more effective antitumor drugs.

Considering that the molecular weight of the fragment crystallizable (Fc) fusion protein is approximately half that of the antibody, it may have better tissue permeability and biologic activity, so Fc fusion drugs targeting CD47 may have different advantages. On the other hand, the recombinant wild-type SIRPα Fc fusion protein TTI-621, which is currently in phase I clinical trials, weakly binds to erythrocytes. However, TTI-621 cannot effectively compete to block the CD47/SIRPα signaling axis owing to low affinity (Petrova et al., 2017). If the affinity of SIRPα targeting CD47 can be artificially increased and the hematotoxicity can be relatively controlled, the therapeutic effect of an SIRPα Fc fusion will be improved to some extent.

Among 10 SIRPα variant forms, SIRPα variant 1 (SIRPα V1) and SIRPα variant 2 comprise approximately 80% of the various types of SIRPα expressed in humans. Similar to the structure of TTI-621, FD164 that targeting CD47 domain is a variant molecule originating from the wild-type SIRPα V1 extracellular Ig-like V type domain and expressed in tandem fusion to the N-terminal region of IgG1 Fc.

Specifically, we combined computer-aided drug design and mammalian cell display technology to conduct in vitro affinity maturation of SIRPα V1. Here, a high-affinity SIRPα variant FD164, with relatively controllable hematologic safety and high antitumor activity, was obtained through high-throughput flow cytometry sorting and biologic evaluation.

Material and Methods

Reagents and Animals. FBS and an ExpiFectamine CHO Transfection Kit were purchased from Life Technologies; jetPRIME-Versatile DNA/siRNA transfection reagent was from Polyplus-transfection; hygromycin B was from Merck; the EndoFree Maxi Plasmid Kit was from Tiangen Biotech (Beijing) Co., Ltd.; restriction enzymes and T4 DNA Ligase were from NEB; KOD-Plus-Neo was from Toyobo, the DNA Miniprep Kit was from QIAGEN; zeocin was from Invitrogen Life Technologies; macrophage colony stimulating factor (M-CSF) was from Peprotech; the FACS Calibur machine was from Becton Dickinson; and carboxyfluorescein succinimidyl ester (CFSE), allophycocyanin (APC)–conjugated anti-human IgG Fc (anti-human IgG Fc-APC), phycoerythrin (PE)–conjugated anti-human IgG Fc (anti-human IgG Fc-PE), APC-conjugated anti-human CD45, APC-conjugated anti-human CD235a, and APC-conjugated anti-human CD14 were from BioLegend. pOG44 and pcDNA5/FRT vectors were obtained from Invitrogen Life Technologies.

The amino acid sequences of SIRPα domain 1 obtained from UniProt [Protein Data Bank (PDB) code: 2UV3] are as follows: ELQVIQPDKSVLVAAGETATLRCTATSLIPVGPIQWFRGAGPGRELIYNQKEGHFPRVTTVSDLTKRNNMDFSIRIGNITPADAGTYYCVKFRKGSPDDVEFKSGAGTELSVRAKPS. Then the SIRPα Fc was generated in which the SIRPα domain 1 was linked to a human IgG1 Fc region. The DNA sequences of Hu5F9 were obtained from publicly available sequences (Liu et al., 2015) and were synthesized and cloned into the IgG4 subtype antibody expression vector pFRT/kIgG4 (modified antibody expression vector with double promoters based on pcDNA5/FRT vector). Next, Hu5F9 was expressed by high-density transient expression system of CHO-S (Gibco, A1369601) and purified by affinity chromatography with protein A agarose. CD47/Fc and CD47/His were obtained from Sino Biologic Inc. (Beijing), and SIRPα-biotin was obtained from ACRO Biosystems Inc. The protein fluorescence labeling service was entrusted to Beijing Jiaxuan Zhirui Biologic Technology Co., Ltd. FACS assay buffer is a mixture of 98% PBS and 2% FBS.

Female NOD-SCID (full strain name: NOD.CB17-Prkdc^{scid}/NcrCrl) mice at 6–8 weeks of age were purchased from Beijing Vital River Biotechnology Co., Ltd., China. Animals were maintained under specific pathogen-free conditions and housed in an air-conditioned room with a light cycle of 12-hour light/12-hour dark and humidity of 40% to 70% in accordance with the animal experimental guidelines set by Animal Ethics Committee of Beijing Institute of Pharmacology and Toxicology. Our animal protocols are approved by the Institutional Animal Care and Use Committee at Beijing Institute of Pharmacology and Toxicology.

All the mice were housed in the independent ventilation cage with five mice per cage and bedded on corncob bedding (Xietong Organism, Jiangsu, China; 1060016). The water source for all animals is sterilized water. Mice standard maintenance diet (Xietong Organism, Jiangsu, China; 1010009) was provided daily in amounts appropriate for the mice. All the mice were monitored daily, and euthanasia was conducted by CO_2 inhalation and confirmed by cervical dislocation when animals exhibited any signs listed in the subsection on B-cell lymphoma xenografts. All the staff conducting procedures related to primary endpoints have obtained laboratory animal training certifications.

Cells and Cell Culture. B-cell lymphoma (Raji, CCL-86) and human embryonic kidney T cells (293T, CRL-11268) were obtained from the American Type Culture Collection (Manassas, VA) and stored in our laboratory. The human non-small cell lung cancer cell lines (PC9) were obtained from the Institute of Biochemistry and Cell Biology of the Chinese Academy of Sciences (Shanghai, China). Flp-In-CHO cells were obtained from Invitrogen Life Technologies. Erythrocytes and peripheral blood mononuclear cells were isolated from whole blood of healthy donors aged 20–40 years and with no restriction on gender. Informed consent was obtained from all donors. Human macrophages were obtained from M-CSF–induced monocytes. Cell lines were not specifically authenticated, but lines were routinely tested and confirmed negative for contamination with mycoplasma. All cell lines described above were grown in RPMI 1640 medium (for Raji) or Dulbecco's modified Eagle's medium (for 293T or PC9) supplemented with 10% FBS, 100 U/ml penicillin, and 100 μg/ml streptomycin. All cells were cultured at 37°C with 5% CO_2.

Computer-Guided Modeling. Based on the crystal structures of human CD47 (PDB code: 2JJS; Hatherley et al., 2008) and SIRPα (PDB code: 2UV3; Hatherley et al., 2007), the coordinates of the hydrogen atoms were assigned, and the whole structures of human CD47 and SIRPα were optimized under the steepest descent (10,000 steps, convergence criterion 0.05 kCal/mol) and conjugate gradient methods (20,000 steps, convergence criterion 0.02 kCal/mol) using consistent valence force field (CVFF). All calculations were performed with Insight II software (2005, MSI Co., San Diego) on an IBM workstation.

Rules for Selecting Key Residues in SIRPα. Based on the theoretical optimized three-dimensional structures of human CD47 and SIRPα, according to the three-dimensional crystal complex structure of human CD47 and high-affinity SIRPα mutant FD6 (PDB code: 4KJY; Weiskopf et al., 2013), the three-dimensional theoretical complex structure of human CD47 and SIRPα was constructed using conformation superimposition and computer-guided molecular docking methods. Furthermore, the three-dimensional predicted complex structure of human CD47 and SIRPα was optimized using the steepest descent (10,000 steps, convergence criterion 0.05 kCal/mol) and conjugate gradient methods (20,000 steps, convergence criterion 0.02 kCal/mol) under CVFF. Upon addressing the distance geometry and computer graphics techniques, the binding domain between human CD47 and SIRPα was analyzed. All calculations were performed with Insight II software (2005, MSI Co., San Diego) on an IBM workstation.

Construction of High-Affinity SIRPα Mutant Library Vectors and Stable Transfection of the Mammalian Cell Library. The open reading frames corresponding of SIRPα V1 domain 1 mutants were amplified by overlapping extension polymerase chain reaction (PCR) and cloned into pFRT-display (the pFRT-display vector is self-constructed from the pcDNA5/FRT Vector to achieve membrane-bound proteins by introducing platelet-derived growth factor receptor transmembrane regions into cloning sites) to construct a SIRPα-pFRT display vector. pOG44 and SIRPα-pFRT-TM (9:1) were co-transfected into Flp-In-CHO cells to generate a mammalian cell library. After 48 hours of transfection, the cells were cultured in Dulbecco's modified Eagle's medium–F12 supplemented with 10% FBS and hygromycin B (1 mg/ml). The surviving cells were pooled together for analysis after 2 weeks.

Fluorescence-Activated Cell Sorting. Three rounds of separation and enrichment were carried out by flow cytometry. A total of 1×10^7 cells were collected and resuspended in FACS assay buffer to a density of 5×10^6 per ml and then stained with APC-conjugated human CD47. The concentrations administered in each round were 10 μg/ml, 5 μg/ml, and 1 μg/ml. They were incubated for 30 minutes at 4°C and then washed twice with FACS assay buffer by centrifugation. Cells were sorted by flow cytometry (FACS Calibur III, Becton Dickinson).

Flow Cytometry Analysis. Cells were washed with FACS assay buffer by centrifugation and suspended in FACS assay buffer. Next, they were stained with FD164 and control proteins for 30 minutes at 4°C, washed and resuspended in FACS assay buffer, followed by detection with APC-conjugated anti-human IgG Fc or PE-conjugated anti-human IgG Fc. Similar to the above experimental method, PC9 cells, Raji cells, erythrocytes, and leukocytes were collected for analysis. The fluorescence was analyzed on the flow cytometry (FACS Calibur II, Becton Dickinson). Data were analyzed by FlowJo 10.5.3 software (Becton Dickinson).

ELISA. An enzyme-labeled array plate was coated with CD47/His (1 μg/ml) at 37°C for 2 hours and then blocked with 1.5% casein at 37°C for 1 hour. The test fusion proteins were diluted with PBS to 15 μg/ml. On this basis, a total of 12 dilution concentrations were obtained by 3-fold serial dilution and added into the appropriate wells, and then the plate was incubated for 1 hour at 37°C. Horseradish peroxidase–conjugated goat anti-human IgG was added to the wells, and the plates were incubated at room temperature for 45 minutes. Binding signals were visualized using 3,3',5,5'-Tetramethylbenzidine (TMB) substrate, and the optical density (OD) was measured at 450 nm.

Competitive ELISA. The enzyme-labeled array plate was coated with CD47/His (1 μg/ml) for 2 hours at 37°C and then blocked with 1.5% casein for 1 hour at 37°C. The test fusion proteins were diluted with biotin-conjugated SIRPα (5 μg/ml) up to 40 μg/ml. On this basis, a total of four dilution concentrations were obtained by 5-fold serial dilution and added into the appropriate wells, and then the plate was incubated for 1 hour at 37°C. Avidin-biotin–conjugated horseradish peroxidase was added to the wells, and the plates were incubated at room temperature for 45 minutes. Binding signals were visualized using 3,3',5,5'-Tetramethylbenzidine (TMB) substrate, and the OD was measured at 450 nm.

Affinity Determination. The bio-layer interferometry technique was used to measure the affinity of the test proteins. The SIRPα mutant fusion protein was captured by anti-human IgG Fc capture and diluted to 10 μg/ml with running buffer for 60 seconds. CD47/His was also diluted to the corresponding concentrations (10 nM, 5 nM, 2.5 nM, 1.25 nM, 0.625 nM, 0.3125 nM, and 0 nM) in running buffer (PBS containing 0.02% Tween-20 and 0.1% bovine serum albumin). The association time of the analyte to CD47/His was set at 180 seconds, the dissociation time was 900 seconds, and chip regeneration was performed with 10 mM Glycine HCl (pH 1.7) solution pulsed at 5 seconds and repeated three times. The data were analyzed with FortéBio Data Analysis software. The measured data were fitted into a 1:1 binding model, and the equilibrium dissociation constant K_D was calculated.

Flow Cytometry–Based Phagocytosis Assay. Monocyte-derived macrophages were extracted from peripheral blood mononuclear cells and cultured for 10 days in growth medium supplemented with 10% FBS and M-CSF (50 ng/ml), and fresh medium with M-CSF was added into culture on day 3. We harvested monocyte-derived macrophages using enzyme-free cell dissociation buffer, and subsequently Raji cells were stained with CFSE for 5 minutes at 37°C. A total of 2×10^5 Raji cells and 2×10^4 monocyte-derived macrophages were cocultured with the test fusion proteins (10 μg/ml) for 4 hours at 37°C. After staining, washed cells were run on the flow cytometry (FACS Calibur II, Becton Dickinson). Data were analyzed by FlowJo 10.5.3 software (Becton Dickinson).

Activity Assay of FD164 Binding to Erythrocytes or Leukocytes. To determine the activity of FD164 binding to erythrocytes and leukocytes, cells were isolated from whole blood and incubated with serial dilutions of FD164, with wild-type SIRPα as the control. PE-conjugated anti-human CD235a or PE-conjugated anti-human CD45 and APC-conjugated anti-human IgG Fc were used as secondary antibody. We used flow cytometry (FACS Calibur II, Becton Dickinson) to assess the binding activity, and these data were analyzed by FlowJo 10.5.3 software (Becton Dickinson).

Hemagglutination Assay. Erythrocytes were isolated from whole blood treated with sodium citrate, followed by several washes with PBS to remove platelets. The suspension of 6% erythrocytes in

PBS was seeded per well in U-bottom 96-well plates. Then, test fusion proteins or PBS was added and incubated overnight at 37°C in 5% CO_2. Wells were graded according to hemagglutination, and images of the plates were saved.

B-Cell Lymphoma Xenografts. Six- to 8-week-old female NOD-SCID mice were maintained in the SPF animal room for 1 week, and the mice did not experience hair loss, weight loss, increased aggressiveness, increased heartbeat and respiratory rate, dehydration, or other abnormalities. After the mice adapted to the feeding environment, 1×10^7 Raji cells were subcutaneously inoculated into the upper groin of the lateral hind limbs of mice. The length and diameter of the tumors were measured with Vernier calipers, and the body weight of the mice was weighed and recorded with an electronic balance. The tumor volume was calculated with the following formula: volume (mm^3) = 0.5× (longest diameter) × (shortest diameter)^2. When the average tumor volume was approximately 250 mm^3, the groups were randomly divided by the table of random numbers according to the tumor volume and the weight of the animals. When the single therapeutic effect was first considered, mice were treated with PBS, FD164 (3 mg/kg), FD164 (10 mg/kg), Hu5F9 (10 mg/kg), SIRPα (10 mg/kg), or SIRPα (3 mg/kg) at 0.2 ml per mouse, two times per week for 3 weeks. When we assessed the antitumor activity of the combination therapy, mice were treated with PBS, FD164 (3 mg/kg), rituximab (5 mg/kg), or FD164 (3 mg/kg) combined with rituximab (5 mg/kg) at 0.2 ml per mouse, two times per week for 3 weeks. Tumor volumes and body weight were also monitored twice weekly. The tumor growth inhibition value was calculated as follows: tumor growth inhibition value (%) = (1 − mean tumor volume of treated group ÷ mean tumor volume of the control) × 100. When the following occurred, mice were euthanized: difficulty in eating and drinking independently, difficulty in standing (up to 24 hours unable to stand or extremely barely able to stand), the tumor metastasizes or grows rapidly to ulceration, causing infection or necrosis, severe breathing difficulties, persistent self-mutilation, unhealed wounds or hypothermia weight rapid loss 15%–20% of its original body weight, loss of appetite for 24 hours, poor appetite (less than 50% of the normal amount) for 3 days or at the end of the study. All the mice in our study were euthanized on the same day (the monotherapy experiment and combination therapy experiment were on day 16 and day 19, respectively), and then the tumor tissues were harvested, weighed, and photographed.

Confirmation of Identified Key Epitopes on CD47. Based on the three-dimensional complex structure of human CD47 and SIRPα, considering the interaction binding mode and the change of the surface distribution between CD47 and SIRPα, three key epitopes of CD47 were predicted using distance geometry and computer graphics method. The key epitopes of CD47 were named CD47-M1 (N^{45}, E^{47}, ^{52}TTEVYVK^{57}, K^{59}), CD47-M2 (D^{64}, T^{67}, D^{69}) and CD47-M3 (^{115}EVTELTRE^{122}, E^{124}), respectively. Dealing with the van der Waals interaction, electrostatic binding, and intermolecular hydrogen bonding, the key residues of the three epitopes of CD47 were substituted with alanine. Then, mutants or wild-type CD47 were engineered and stably expressed on the surface of the Flp-In-CHO cell line. Finally, we measured the binding activities of the ectopic CD47 proteins to FD164 by flow cytometry. The data were analyzed using FlowJo 10.5.3 software (Becton Dickinson).

Statistical Analysis. Power was performed in G*Power (Version 3.1.9.7, University Düsseldorf, Germany) (Faul et al., 2007). A post hoc power analysis of the achieved power indicated that for a single-drug treatment animal experiment, a sample size of five enables moderate power (power = 0.88) to detect a statistical difference; for a combination therapy animal experiment, the power was 0.82.

When comparing multiple groups, data were analyzed by one-way ANOVA followed by Tukey's test. The statistical significance of tumor volume and tumor weight differences between groups at the end of treatment was determined by one-way ANOVA followed by Tukey's test. Specific statistical analysis methods indicated in the figure legends where results are presented. Data were considered statistically significant when P values lower than 0.05. Aside from the ELISA and competitive ELISA results, all error bars display the S.E.M. All in vitro experiments were replicated at least three times. All data were analyzed using Prism software (version 8.0, GraphPad, San Diego, CA).

Results

High-Affinity SIRPα Mutant Library Design Based on Computer Structure Prediction. To investigate the binding mode in detail between human CD47 and SIRPα theoretically, the three-dimensional structures of human CD47, SIRPα, and their complex should be analyzed using theoretical method under suitable molecular force field at first. Dealing with computer-guided molecular modeling and minimizing methods, the theoretical three-dimensional structures of human CD47 and SIRPα were obtained and shown in Fig. 1A, B. Based on the template structure of human CD47 and SIRPα mutant FD6 (PDB code: 4KJY), the minimized three-dimensional complex structure of human CD47 and SIRPα is

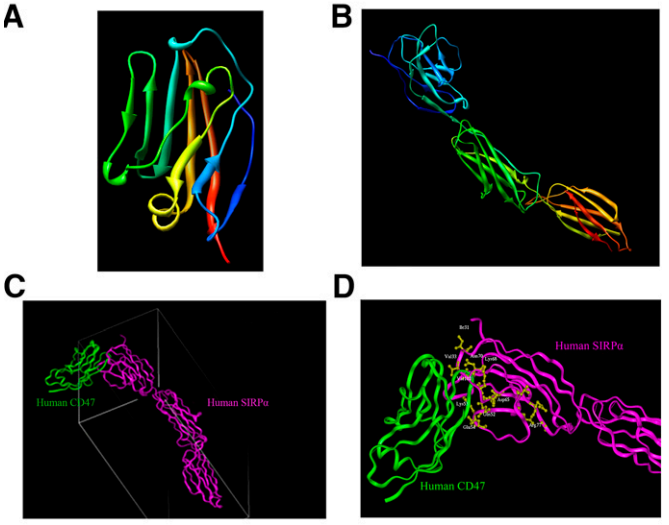

E

ELQVIQPDKSVLVAAGETATLRCTATSLIPVGPIQWFRGA
GPGRELIYNQKEGHFPRVTTVSDLTKRNNMDFSIRIGNI
TPADAGTYYCVKFRKGSPDDVEFKSGAGTELSVRAKPS

Fig. 1. Design and identification of high-affinity SIRPα variants using computer-aided drug design. (A) The three-dimensional theoretical ribbon structure of the human CD47 extracellular ribbon optimized with CVFF derived from its crystal structure (PDB code: 2JJS). (B) The three-dimensional theoretical ribbon structure of the SIRPα extracellular region optimized with CVFF. It was shown that the human SIRPα extracellular segment has three domains, one immunoglobulin-like V domain (I) and two immunoglobulin-like C domains (II and III), derived from its crystal structure (PDB code: 2UV3). (C) The three-dimensional theoretical ribbon complex structure of human CD47 and SIRPα extracellular region, where the green ribbon denotes the main chain carbon atom orientation of human CD47 and the pink denotes the main chain carbon atom orientation of SIRPα extracellular region. (D, E) The important amino acid residues of SIRPα extracellular region identified by CD47 predicted based on the three-dimensional theoretical structure of human CD47 and SIRPα extracellular region using computer graphics and distance geometry method. The green ribbon structure denotes the main chain carbon atom orientation of human CD47, the pink denotes the main chain carbon atom orientation of SIRPα extracellular region, and the yellow ball and sticks denote the important residues of SIRPα extracellular region identified by human CD47. The red residues represent key amino acid of SIRPα involved in the recognition of CD47.

shown in Fig. 1C. Considering the intermolecular interaction, the key amino acid residues of human SIRPα [sequences are derived from SwissProt database P78324 (SHPS1_Human); the amino acid sequence is from E^{33} to S^{149}] that participate in the binding to CD47 were determined, and the binding mode between the key residues of human SIRPα and CD47 was analyzed theoretically (Fig. 1D, E). The residues Ile61, Val63, Val93, Leu96, and Val142 of human SIRPα are involved in hydrophobic interactions, whereas the residues Glu77, Gln82, Lys83, Glu84, Asp95, Asn100, Arg107, and Gly109 are involved in hydrophilic binding. Specifically, the residues Gln82, Lys83, Glu84, Asp95, Lys98, and Asn100 formed intermolecular hydrogen bonds with residues on human CD47. With the predicted binding mode between human CD47 and SIRPα, a virtual mutant library that might have higher affinity than the wild-type SIRPα protein was constructed.

Directed Evolution of High-Affinity SIRPα V1 with the Epitope-Specific Cell Library. High affinity is an important prerequisite for effectively blocking the CD47-SIRPα interaction; thus, higher affinity SIRPα variants could function as a decoy to block the CD47-SIRPα interaction. According to the computer simulation results, we determined the 14 key amino acid sites of the "contact residue" library with possible amino acid variants that can theoretically increase the affinity between SIRPα and CD47 (Table 1). The DNA sequences of SIRPα mutants were amplified, and the electrophoresis assay showed that the right lane had the appropriate DNA fragment length (~434 base pairs) (Fig. 2A) as generated by overlap PCR, and the mutated-sites sequences were inserted into the library vector.

To confirm the quality of the SIRPα mutant library, library sequencing was carried out. A total of 76 positive clones were obtained after sequencing clones. We performed diversity analysis and cluster analysis of the sequencing results. The results elucidate that the 76 sequences had a certain homology on the evolutionary tree and had no identical sequence (Supplemental Fig. 1A), indicating that the constructed SIRPα mutant molecular library was diverse. At the same time, all the mutation sites were located at predicted sites and the mutant amino acids were consistent with the theoretically designed amino acids; the actual frequency of occurrence was basically consistent with the theoretical design (Supplemental Fig. 1B). These results suggested that an SIRPα mutant library was successfully constructed.

TABLE 1
Table of positions of the contact residue library with possible amino acid mutant sites that can theoretically increase affinity between SIRPα and CD47

Key amino acid residues	Substitutions
I61	I, V, F
V63	V, I, L, F
E77	E, S, V, L
Q82	Q, E, S, N
K83	K, R, Q
E84	E, R, N, S, D
V93	V, I, L
D95	D, E, N, S
L96	L, T, S
K98	K, R
N100	N, D, E
R107	R, K, S, Q
G109	G, S, Q, N
V142	V, I, L, S, T

Screening and Identification of High-Affinity SIRPα Candidates Using Mammalian Cell Libraries. The library plasmids with millions of SIRPα mutants were transfected into Flp-In-CHO cells. Three consecutive rounds of cytometry sorting were conducted to screen for high-affinity SIRPα mutants, after which the clones with high binding activities were enriched with the positive rate ranging from 47.3% to 80.5% (Fig. 2B). Twenty high-affinity SIRPα mutants with different amino acid sequences were selected using flow cytometry and sequencing analysis. These 20 SIRPα mutants were fused to IgG1 Fc and expressed by transient transfection of 293T cells, and the ability of these candidate fusion proteins binding to CD47 was then assessed by ELISA. As shown in Supplemental Figure 1C, the candidate molecules, namely, 121, 148, 164, 2734, 2738, 2740, and 2744, show better binding activity to CD47 than the wild-type SIRPα.

To further screen out the best SIRPα variant fusion protein, seven candidate proteins were prepared, expressed in 293T cells, and purified by affinity chromatography with protein A agarose. The ELISA results confirmed that a descending order of binding strength starting with 121 followed by 164, 2740, 2744, 2738, 2734, and 148 (Fig. 2C), and the specific data values are correspondingly shown in Table 2. Then, we compared the binding activity of the seven candidate proteins to red blood cells by flow cytometry. As indicated in Supplemental Figure 1D, the result shows that the order of binding activity is 121 > 2740 > 2738 > 164 > 2734 > 2744 > 148. Considering its binding activities to CD47 and red blood cells, 164, which has the relatively high binding activity to CD47 and moderate binding activity to red blood cells, was selected for further study and renamed FD164.

Characterization of the High-Affinity SIRPα Fusion Protein FD164. The amino acid differences at the mutation site of wild-type SIRPα and FD164 are shown in Table 3. First, the purity of purified FD164 was analyzed by SDS-PAGE. The results of reduced and nonreduced SDS-PAGE showed that the molecular weight of the fusion protein was approximately 100 kDa, and the purity of the protein was greater than 95% (Supplemental Fig. 2A, B). To characterize FD164, we determined its binding activity to CD47 and ability to block the CD47-SIRPα interaction by ELISA and flow cytometry. The results suggested that FD164 binds to CD47 (Fig. 3A) in a dose-dependent manner, with an EC_{50} value of 0.04 ± 0.01 nM, whereas the EC_{50} value of wild-type SIRPα was 0.6 ± 0.1 nM. We used flow cytometry to detect the binding activity of CD47 on tumor cell surface (PC9 and Raji cell lines). The results confirmed that FD164 can bind to CD47 on tumor cell surface (Supplemental Fig. 2C, D). Competitive ELISA results showed FD164 inhibits the CD47-SIRPα interaction, which is better than wild-type SIRPα (Fig. 3B). According to the flow cytometry results, FD164 blocked SIRPα binding to CD47 on the cell surface; specifically, FD164 fully inhibited the CD47-SIRPα interaction at low concentrations (1.25 μg/ml), which implies that its inhibitory activity is similar to that of Hu5F9. By contrast, wild-type SIRPα can only inhibit 20% at the same concentration (Fig. 3C).

Next, other in vitro activities of FD164 were also determined, including affinity and induction of tumor cell

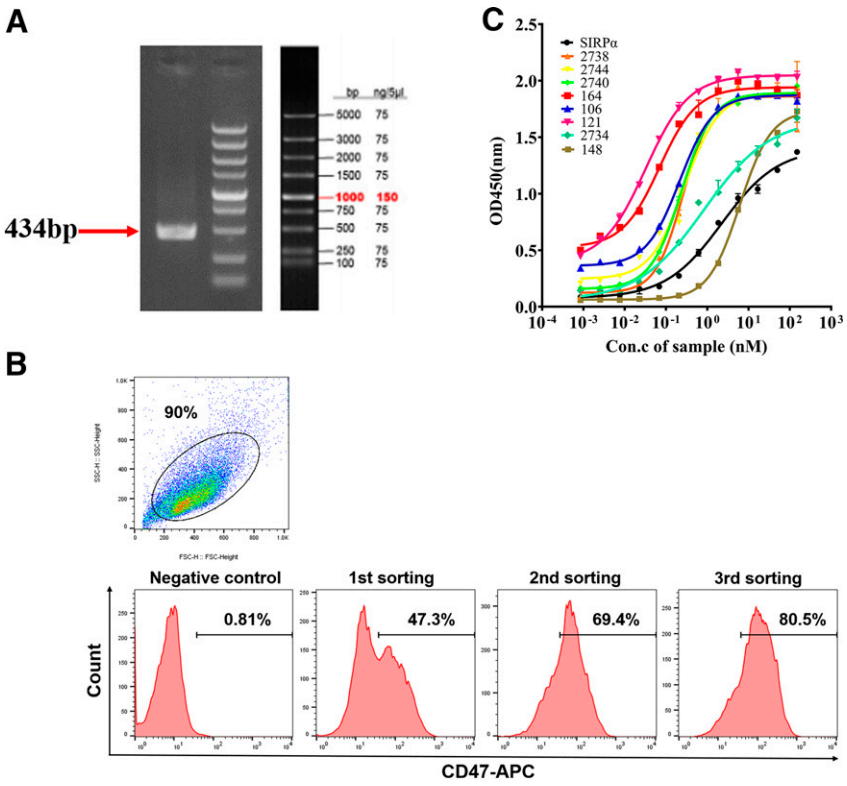

Fig. 2. Library construction and selection. (A) The segments of the SIRPα molecular library DNA fragments were amplified by PCR and quantified by gel electrophoresis. The SIRPα extracellular segment has 434 base pairs (bp) in theory, and the gel results are consistent with the theoretical predictions. (B) FACS of Flp-InTM-CHO cells expressing SIRPα candidates that strongly bound to CD47. Three rounds of cytometry sorting were performed to obtain high-affinity SIRPα cell clones. (C) The binding activity of SIRPα candidates to CD47 was determined by ELISA.

phagocytosis. From the affinity assay results, the K_D value of wild-type SIRPα was higher than that of FD164 (0.3 ± 0.1 nM versus 0.06 ± 0.02 nM), which indicates that the affinity of FD164 is higher than that of wild-type SIRPα (Fig. 3D, E). We then assessed the ability of FD164 to promote macrophage-mediated phagocytosis of Raji cells using flow cytometry. From the results of the in vitro phagocytosis experiments (Fig. 3F, G), FD164 promoted macrophage phagocytosis of CFSE-labeled Raji cells compared with that promoted by SIRPα, and even has a tendency to be better than Hu5F9. All these results suggest that FD164 exhibits higher specificity, affinity, and activity than wild-type SIRPα.

FD164 Inhibited Tumor Growth In Vivo. We evaluated the antitumor effects of monotherapy with FD164 in a xenograft NOD-SCID mouse model of human Burkitt's lymphoma. When the average tumor volume reached 250 mm^3, five mice with the largest or smallest tumor volume were excluded, so 30 mice were included in the experimental group. Then, 30 tumor-bearing mice were randomized into six groups ($n = 5$). We administered FD164 intraperitoneally and monitored tumor growth. During the administration process, none of the mice had accidents (sudden weight loss, etc.). There were no exclusions and a total of 30 animals included in the analysis of the antitumor effect. The results show that FD164 effectively inhibit the growth of tumor in a dose-dependent manner. The tumor growth of the mice treated with FD164 (10 mg/kg) was significantly slower than that of the other five groups. The tumor growth inhibition value (TGI) in the FD164 (10 mg/kg) group was 79.40%, which was similar to that in the Hu5F9 (10 mg/kg) group and higher than that in the SIRPα (10 mg/kg) group, and the difference in tumor volume was statistically significant difference at day 16 (Fig. 4A). Consistent with tumor volume, the tumor weight of the FD164 group was significantly smaller than that of the SIRPα group at the same dose (Fig. 4B). Figure 4C is a picture of excised tumors, which intuitively shows the antitumor effect of FD164. The body weight of the mice did not change significantly during drug administration (Fig. 4D). These results suggest that monotherapy with FD164 slowed the growth of tumor and have stronger antitumor effect than wild-type SIRPα.

Given that drugs targeting CD47 have a synergistic effect when combined with other drugs, we also evaluated the antitumor effect of rituximab combined with FD164 in the xenograft NOD-SCID mouse model of human Burkitt's lymphoma.

TABLE 2
The OD values and EC_{50} values of candidate molecules tested by ELISA

Value	SIRPα	148	2738	2744	2740	164	121	2734
Bottom	0.08	0.06	0.12	0.24	0.16	0.52	0.40	0.05
Top	1.40	1.74	1.86	1.88	1.89	1.94	2.05	1.67
Hill slope	0.64	1.14	1.31	1.06	1.14	0.96	0.83	0.54
EC_{50} (nM)	2.26	6.13	0.26	0.28	0.24	0.07	0.03	0.84

The OD values and EC_{50} values in this table are the detailed presentation of Fig. 2C. The experiments were replicated at least in triplicate, and one of three experiments is shown. Data are presented as means ± S.D.

TABLE 3
Amino acid sequence information of FD164

Sample	Mutation site													
	61	63	77	82	83	84	93	95	96	98	100	107	109	142
WT allele 1	I	V	E	Q	K	E	V	D	L	K	N	R	G	V
FD164	F	I	L	Q	R	S	V	E	T	K	D	Q	S	I

WT, wild type.

When the average tumor volume reached 250 mm^3, four mice with the largest or smallest tumor volume were excluded. Then, 20 tumor-bearing mice were randomized into four groups ($n = 5$). There were no exclusions, and a total of 20 animals were therefore included in the analysis of the antitumor effect. The result suggested the growth of tumor in the combination therapy group was relatively slower than in the other three groups. Compared with the PBS control group, the TGI of rituximab (5 mg/kg) was only 5.06%, and the TGI of FD164 (3 mg/kg) was 47.30%. Notably, the TGI of FD164 (3 mg/kg) and rituximab (5 mg/kg) combination therapy was 69.80%. The results show that FD164 combined with rituximab can significantly enhance the tumor-suppressive activity of rituximab ($P < 0.01$) (Fig. 5). Collectively, these in vivo data suggest that FD164 elicited potential antitumor activity and can produce a superior effect to the administration with rituximab of a single therapy.

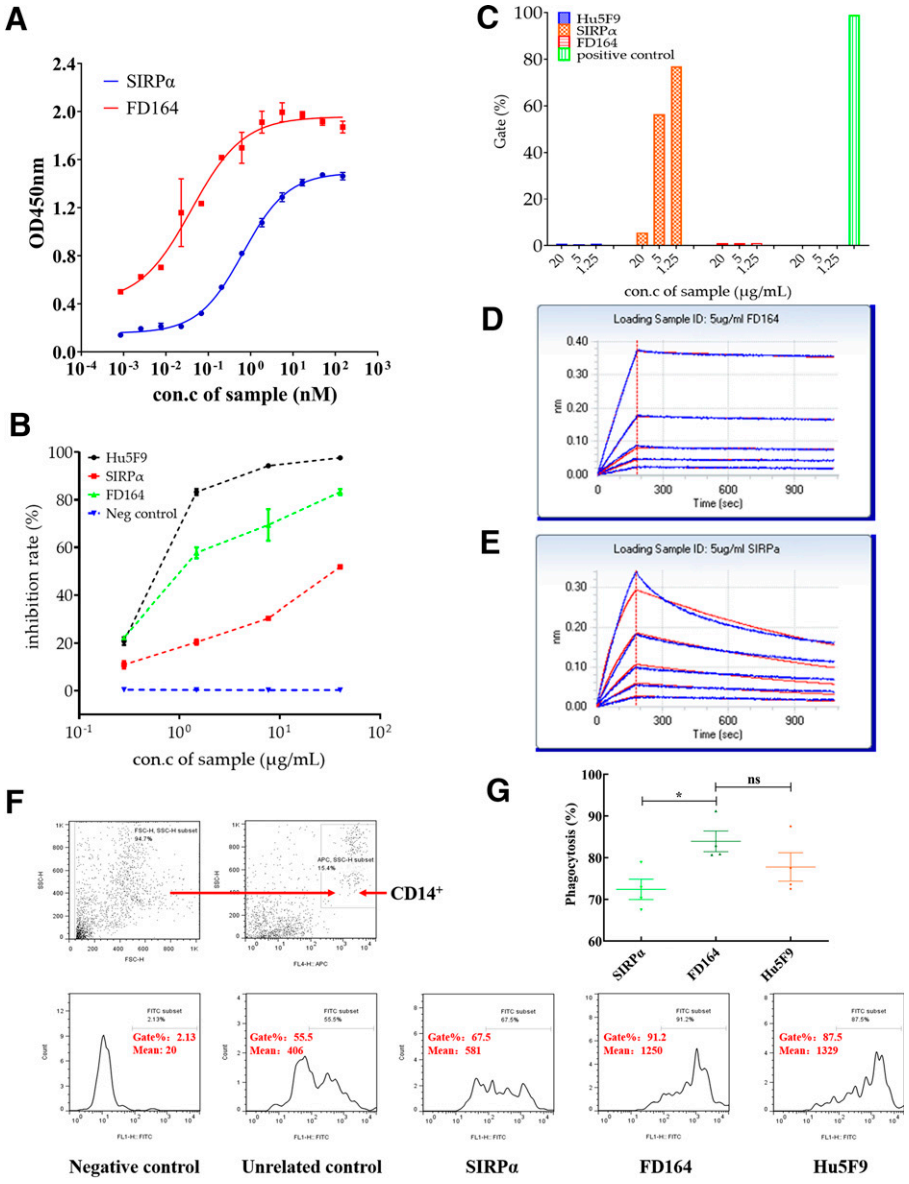

Fig. 3. Characterization of the high-affinity SIRPα variant fusion FD164. (A) The activity of FD164 binding to CD47 was determined by ELISA. (B) The activity of FD164 blocking the interaction between CD47 and SIRPα was assessed by ELISA. (C) The activity of FD164 blocking the interaction between CD47 and SIRPα was assessed by flow cytometry. (D) The affinity of SIRPα to CD47 was measured using bio-layer interferometry with FortéBio. (E) The affinity of FD164 to CD47 was measured using bio-layer interferometry with FortéBio. (F, G) FD164 promotes macrophage-mediated phagocytosis of Raji cells in vitro. A representative experiment out of four independent experiments is shown. ns, no significance; *, $P < 0.05$; **, $P < 0.01$; ***, $P < 0.001$ versus control.

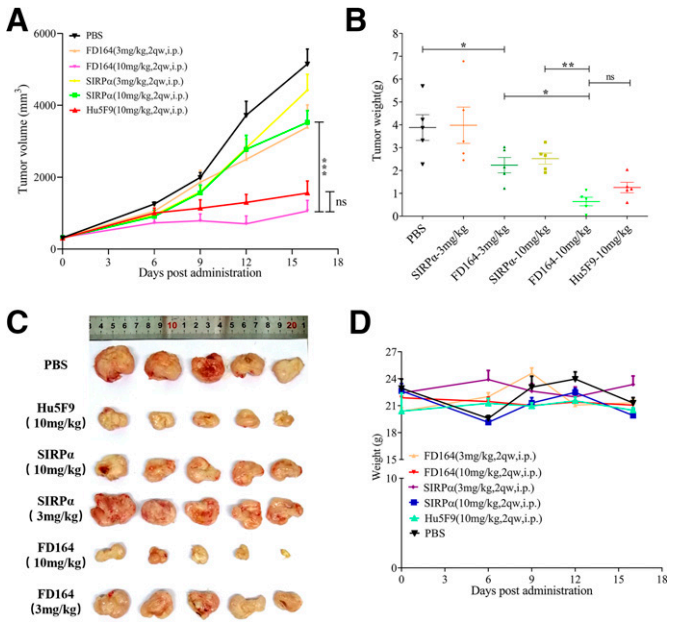

Fig. 4. FD164 exhibits high antitumor activity in a human Burkitt's lymphoma cell tumor xenograft model in mice. (A) Raji cells were subcutaneously transplanted into NOD-SCID mice, and the tumor-bearing mice were treated with a low (3 mg/kg) and high (10 mg/kg) dose of FD164, a low (3 mg/kg) and high (10 mg/kg) dose of SIRPα, or a high (10 mg/kg) dose of Hu5F9 as a positive control with the PBS as a negative control ($n = 5$). Tumor growth curves are shown as relative tumor volume. Statistical significance (on day 16) was calculated by one-way ANOVA with Tukey test. $P \leq 0.05$ was considered to be statistically significant. (B) Tumor weights of each group were measured after tumor excision. Statistical significance was calculated by one-way ANOVA with Tukey test. $P \leq 0.05$ was considered to be statistically significant. (C) The image of the excised tumor tissues from all mice in each group. (D) Mouse weights were measured and are shown in the graph. Data are presented as means ± S.E.M. ns, no significance; *, $P < 0.05$; **, $P < 0.01$; ***, $P < 0.001$ versus control. 2qw, twice a week.

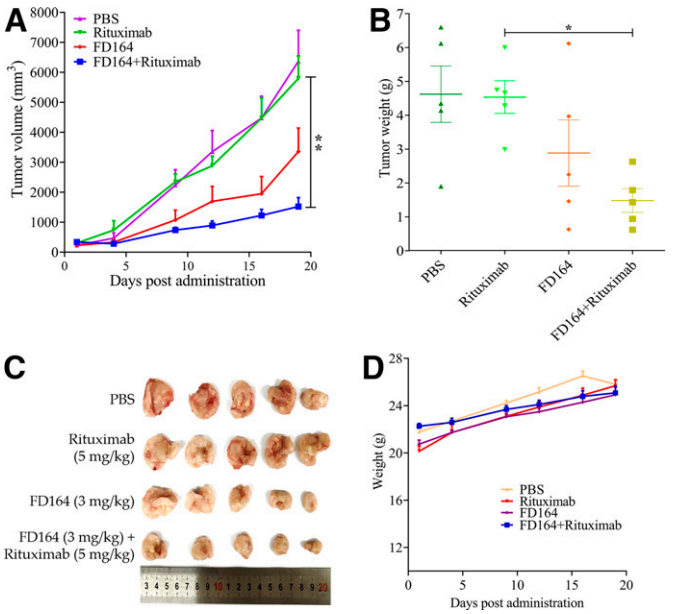

Fig. 5. FD164 combined with rituximab exhibits high antitumor activity in human Burkitt's lymphoma cell tumor-engrafted mouse models. (A) Raji cells were subcutaneously transplanted into NOD-SCID mice, and the tumor-bearing mice were treated with FD164 (3 mg/kg), rituximab (5 mg/kg), or FD164 (3 mg/kg) combined with rituximab (5 mg/kg) or PBS as a negative control ($n = 5$). Tumor volumes were measured, and the average volume is shown. Statistical significance (on day 19) was calculated by one-way ANOVA with Tukey test. $P \leq 0.05$ was considered to be statistically significant. (B) Tumor weights of each group were measured after tumor excision. Statistical significance was calculated by one-way ANOVA with Tukey test. $P \leq 0.05$ was considered to be statistically significant. (C) The image of the excised tumor tissues from all mice in each group. (D) Mouse weights were measured and are shown in the graph. Data are presented as means ± S.E.M. ns, no significance; *, $P < 0.05$; **, $P < 0.01$; ***, $P < 0.001$ versus control.

FD164 Shows More Favorable Hematologic Safety. CD47 is widely expressed on the surface of erythrocytes, and the results of multiple clinical trials suggest that CD47-targeted drugs may cause anemia. Therefore, assessing the risk of FD164-induced anemia has importance. So, we verified the effect of FD164 on erythrocyte agglutination. As shown in Fig. 6A, hemolysis occurred in the Hu5F9 group at 12.5 μg/ml, but there was no hemolysis in any concentrations of FD164 and SIRPα. The results show that FD164 does not affect blood agglutination at concentrations up to 100 μg/ml. We also compared the binding activity of FD164 and Hu5F9 with erythrocytes, and the median fluorescence intensity of FD164 at high concentrations (50 μg/ml) was even lower than that of Hu5F9 at low concentrations (0.5 μg/ml) (Fig. 6B). These data indicated that FD164 showed lower binding activity to erythrocytes in comparison with Hu5F9. In similar, FD164 was tested with potential binding activity to erythrocytes ($CD235a^+$) and white blood cells ($CD45a^+$). The results showed that the binding activity of FD164 with blood cells was weaker than Hu5F9, slightly stronger than SIRPα (Fig. 6C). In summary, we confirmed that FD164 caused no obvious hematologic toxicity and is even better than that of clinical research drug Hu5F9 in vitro.

Confirmation of FD164 Recognized Key Epitopes. Different epitopes of the same target molecule may affect the biologic function of the drug. Computer predicts that FD164 recognizes the key epitopes of CD47 and 3 CD47 mutants were displayed on the surface of mammalian cell. The flow cytometry results showed that CD47-M1 and CD47-M3 could bind to neither wild-type SIRPα nor FD164 (Fig. 7). The above results indicate that the N^{45}, E^{47}, ^{52}TEVYVK^{58}, K^{60}, ^{115}EVTELTRE^{122}, and E^{124} residues are the key recognition epitopes and there is no obvious difference between the residues recognized by FD164 and those by wild-type SIRPα. Therefore, compared with wild-type SIRPα, the epitope that recognized by FD164 had no significant drift.

Discussion

With the in-depth exploration of the mechanism and function of CD47, it is becoming clearer that innate immune checkpoint molecules play a key role in many tumors escaping the immune system response. Therefore, blocking the CD47-SIRPα interaction has been indicated to potentially inhibit tumor progression (Hazama et al., 2020; Kauder et al., 2018; Veillette and Chen, 2018). However, CD47 is widely distributed in normal human tissues (especially in blood as represented by red blood cells), which causes certain obstacles to the clinical application of antibody-based treatments. First, drugs targeting CD47 through intravenous injection into the blood circulation will quickly bind to red blood cells, platelets, etc. and rapidly reduce the number of

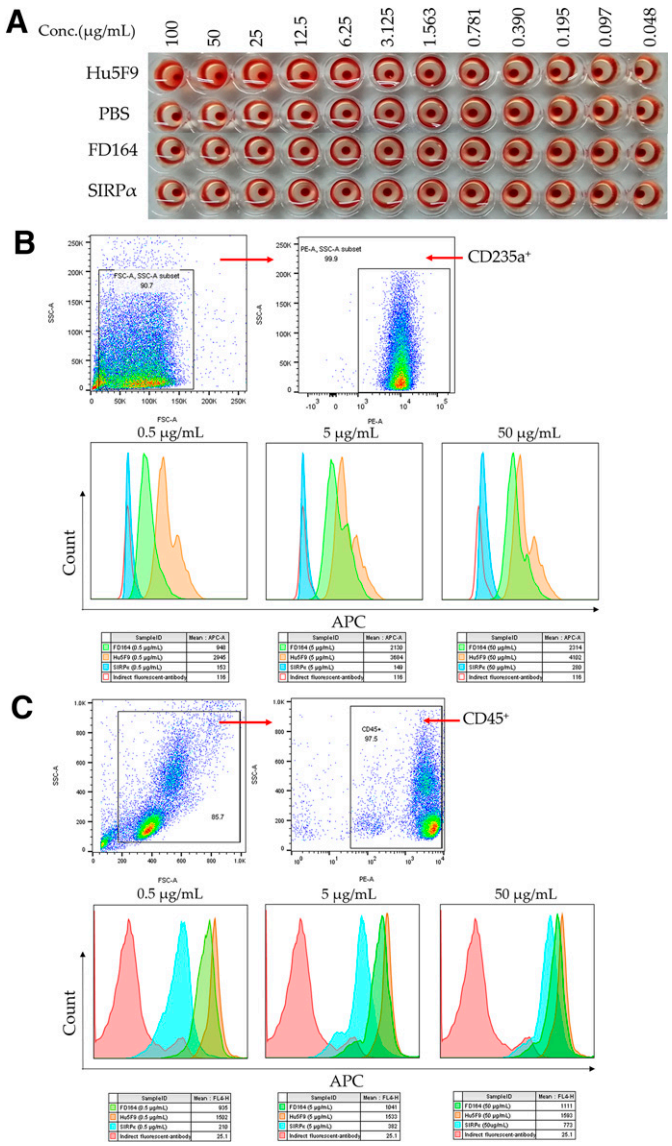

Fig. 6. FD164 shows medium affinity to human red blood cells and leukocytes. (A) The effect of FD164 on hemagglutination, with Hu5F9 and SIRPα as controls. Experiments were independently repeated at least three times, and one representative experiment is shown. (B) The activity of FD164 binding to human red blood cells was determined by flow cytometry. (C) The activity of FD164 binding to leukocytes was determined by flow cytometry.

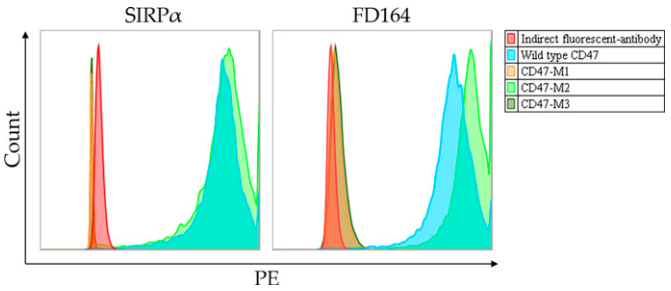

Fig. 7. Confirmation of the key epitopes of CD47 recognized by FD164. Determination of the binding activity of SIRPα or FD164 with wild-type CD47 and CD47 mutants (CD47-M1, CD47-M2, CD47-M3) expressed on the surface of Flp-In-CHO cells by flow cytometry.

viable red blood cells or platelets, resulting in hemolysis or thrombocytopenia. Second, blood cells are equivalent to a tremendous "antigen sink," and drugs must be injected at a larger dose to achieve higher receptor occupancy on the tumor to exert an antitumor effect. Therefore, hematologic toxicity usually defines clinically safe doses. To solve these problems, many pharmaceutical companies have developed different clinical strategies. For example, Hu5F9, developed by Forty Seven, is administered in a stepwise manner. In the clinical trials of Hu5F9 combined with rituximab for the treatment of diffuse large B-cell lymphoma and follicular lymphoma, the investigators first adopted a low dose (1 mg/kg) to eliminate senescent red blood cells and induce red blood cell regeneration. After the body is compensatively tolerant to a low dose of the drug, a maintenance dose (10–30 mg/kg) is administered to avoid the occurrence of anemia (Advani et al., 2018). TTI-621, a wild-type SIRPα Fc fusion protein, constructed by Trillium Therapeutic (Petrova et al., 2017), shows minimal binding to red blood cells but elicits clinical adverse reactions of thrombocytopenia. To better reduce the systemic toxicity of this drug and enhance its efficacy, in clinical studies on relapsed or refractory mycosis fungoides and Sézary syndrome, researchers administered TTI-621 locally by percutaneous injection. The results revealed that TTI-621 was well tolerated, and 91% (20/22) of patients with mycosis fungoides showed significant improvement in local lesions, with some even showing distal and systemic therapeutic effects. However, from the current clinical data, because the maximum dose of TTI-621 is 2 mg/kg, it is difficult to achieve effective surface receptor occupancy on the tumor, especially for the treatment of solid tumors. Similar to this study, ALX Oncology used yeast display to obtain a high-affinity SIRPα named ALX148 that can target CD47 more effectively. Considering the pharmacokinetic properties and the long half-life of Fc fusion protein drugs, ALX Oncology adopted a differentiated Fc design by mutating Fc (L234A; L235A; G237A; N297A) to inactivate Fc-mediated antibody-dependent cell-mediated cytotoxicity and complement-dependent cytotoxicity, which greatly increases the maximum clinical dose to 30 mg/kg. Currently, ALX148, combined with trastuzumab or pembrolizumab, has produced a very good curative effect in the clinical aspect (Kauder et al., 2018).

In this study, based on computer-aided design and a mammalian cell antibody library, we carried out affinity maturation of the SIRPα V1 variant FD164. This technology platform has advantages for screening antibodies or fusion proteins with high biologic activity. First, computer-aided drug design is a popular technique for drug development in the efficient calculation and analysis of drug interactions because computers can perform structure simulation and molecular docking of specific drug groups or macromolecular proteins (Cao et al., 2020; Qiao et al., 2013). Specifically, in the development of antibodies and protein drugs, with the help of computer homology modeling and molecular docking modules, it is possible to effectively construct protein-protein (e.g., ligand-receptor, antigen-antibody) mutual recognition pattern and obtain structural information (Duan et al., 2019; Qiao et al., 2013). Combined with the design of a virtual library based on this structural information, a molecular

library with a small capacity and high quality can effectively guide in vitro evolution. Second, the mammalian cell library utilizes the commonly used CHO cell line for antibody selection. Invitrogen has carried out genetic engineering with CHO cells and finally obtained a targeted integration cell system. Using this system, the selected antibodies or protein drugs can be seamlessly connected to industrial production, with good applicability and a high success rate (Duan et al., 2019; Luo et al., 2018). In a short, we used computer-aided design combined with mammalian cell-surface display technology to design and screen high-affinity SIRPα variant fusion proteins. After high-throughput flow cytometry sorting and preliminary activity evaluation, FD164, which specifically targets CD47 with higher activity, was identified. Compared with wild-type SIRPα, FD164 has higher affinity to CD47, blocking the CD47-SIRPα interaction more effectively, and can better promote macrophage phagocytosis of tumor cells in vitro. Single-drug or combination therapy in vivo has a stronger antitumor effect. In summary, FD164 has promising prospects for application.

Acknowledgments

The authors thank Springer Nature Group (https://authorservices.springernature.com/) for editing a draft of this manuscript.

Authorship Contributions

Participated in research design: Z. Wang, Feng, Peng, Luo.

Conducted experiments: Z. Wang, Qiao, J. Wang, Zhou, Wu, Zhang.

Contributed new reagents or analytical tools: H. Wang, Feng, Shen.

Performed data analysis: Hu, Li.

Wrote or contributed to the writing of the manuscript: Z. Wang, Ren, Chen, Peng, Luo.

References

Advani R, Flinn I, Popplewell L, Forero A, Bartlett NL, Ghosh N, Kline J, Roschewski M, LaCasce A, Collins GP et al. (2018) CD47 blockade by Hu5F9-G4 and rituximab in non-Hodgkin's lymphoma. *N Engl J Med* **379**:1711–1721.

Banchereau J and Palucka K (2018) Immunotherapy: cancer vaccines on the move. *Nat Rev Clin Oncol* **15**:9–10.

Barclay AN and Brown MH (2006) The SIRP family of receptors and immune regulation. *Nat Rev Immunol* **6**:457–464.

Barrera L, Montes-Servín E, Hernandez-Martinez J-M, García-Vicente MLÁ, Montes-Servín E, Herrera-Martínez M, Crispín JC, Borbolla-Escoboza JR, and Arrieta O (2017) CD47 overexpression is associated with decreased neutrophil apoptosis/phagocytosis and poor prognosis in non-small-cell lung cancer patients. *Br J Cancer* **117**:385–397.

Belgiovine C, D'Incalci M, Allavena P, and Frapolli R (2016) Tumor-associated macrophages and anti-tumor therapies: complex links. *Cell Mol Life Sci* **73**:2411–2424.

Cao L, Goreshnik I, Coventry B, Case JB, Miller L, Kozodoy L, Chen RE, Carter L, Walls AC, Park YJ et al. (2020) De novo design of picomolar SARS-CoV-2 miniprotein inhibitors. *Science* **370**:426–431.

Chao MP, Majeti R, and Weissman IL (2011) Programmed cell removal: a new obstacle in the road to developing cancer. *Nat Rev Cancer* **12**:58–67.

Darvin P, Toor SM, Sasidharan Nair V, and Elkord E (2018) Immune checkpoint inhibitors: recent progress and potential biomarkers. *Exp Mol Med* **50**:1–11.

Duan Y, Luo L, Qiao C, Li X, Wang J, Liu H, Zhou T, Shen B, Lv M, and Feng J (2019) A novel human anti-AXL monoclonal antibody attenuates tumour cell migration. *Scand J Immunol* **90**:e12777.

Eggermont AM, Chiarion-Sileni V, Grob JJ, Dummer R, Wolchok JD, Schmidt H, Hamid O, Robert C, Ascierto PA, Richards JM et al. (2016) Prolonged survival in stage III melanoma with ipilimumab adjuvant therapy. *N Engl J Med* **375**:1845–1855.

Eggermont AMM, Chiarion-Sileni V, Grob J-J, Dummer R, Wolchok JD, Schmidt H, Hamid O, Robert C, Ascierto PA, Richards JM et al. (2015) Adjuvant ipilimumab versus placebo after complete resection of high-risk stage III melanoma (EORTC 18071): a randomised, double-blind, phase 3 trial. *Lancet Oncol* **16**:522–530.

Faul F, Erdfelder E, Lang AG, and Buchner A (2007) G*Power 3: a flexible statistical power analysis program for the social, behavioral, and biomedical sciences. *Behav Res Methods* **39**:175–191.

Galli S, Zlobec I, Schürch C, Perren A, Ochsenbein AF, and Banz Y (2015) CD47 protein expression in acute myeloid leukemia: a tissue microarray-based analysis. *Leuk Res* **39**:749–756.

Hatherley D, Graham SC, Turner J, Harlos K, Stuart DI, and Barclay AN (2008) Paired receptor specificity explained by structures of signal regulatory proteins alone and complexed with CD47. *Mol Cell* **31**:266–277.

Hatherley D, Harlos K, Dunlop DC, Stuart DI, and Barclay AN (2007) The structure of the macrophage signal regulatory protein alpha (SIRPalpha) inhibitory receptor reveals a binding face reminiscent of that used by T cell receptors. *J Biol Chem* **282**:14567–14575.

Hazama D, Yin Y, Murata Y, Matsuda M, Okamoto T, Tanaka D, Terasaka N, Zhao J, Sakamoto M, Kakuchi Y et al. (2020) Macrocyclic peptide-mediated blockade of the CD47-SIRPα interaction as a potential cancer immunotherapy. *Cell Chem Biol* **27**:1181–1191.e7.

Kauder SE, Kuo TC, Harrabi O, Chen A, Sangalang E, Doyle L, Rocha SS, Bollini S, Han B, Sim J et al. (2018) ALX148 blocks CD47 and enhances innate and adaptive antitumor immunity with a favorable safety profile. *PLoS One* **13**:e0201832.

Kaur S, Elkahloun AG, Singh SP, Chen Q-R, Meerzaman DM, Song T, Manu N, Wu W, Mannan P, Garfield SH et al. (2016) A function-blocking CD47 antibody suppresses stem cell and EGF signaling in triple-negative breast cancer. *Oncotarget* **7**:10133–10152.

Koh E, Lee EJ, Nam GH, Hong Y, Cho E, Yang Y, and Kim IS (2017) Exosome-SIRPα, a CD47 blockade increases cancer cell phagocytosis. *Biomaterials* **121**:121–129.

Labanieh L, Majzner RG, and Mackall CL (2018) Programming CAR-T cells to kill cancer. *Nat Biomed Eng* **2**:377–391.

Liu J, Wang L, Zhao F, Tseng S, Narayanan C, Shura L, Willingham S, Howard M, Prohaska S, Volkmer J et al. (2015) Pre-clinical development of a humanized anti-CD47 antibody with anti-cancer therapeutic potential. *PLoS One* **10**:e0137345.

Luo L, Wang S, Lang X, Zhou T, Geng J, Li X, Qiao C, Feng J, Shen B, Lv M et al. (2018) Selection and characterization of the novel anti-human PD-1 FV78 antibody from a targeted epitope mammalian cell-displayed antibody library. *Cell Mol Immunol* **15**:146–157.

Ma L, Zhu M, Gai J, Li G, Chang Q, Qiao P, Cao L, Chen W, Zhang S, and Wan Y (2020) Preclinical development of a novel CD47 nanobody with less toxicity and enhanced anti-cancer therapeutic potential. *J Nanobiotechnology* **18**:12.

Matlung HL, Szilagyi K, Barclay NA, and van den Berg TK (2017) The CD47-SIRPα signaling axis as an innate immune checkpoint in cancer. *Immunol Rev* **276**:145–164.

O'Donnell JS, Long GV, Scolyer RA, Teng MW, and Smyth MJ (2017) Resistance to PD1/PDL1 checkpoint inhibition. *Cancer Treat Rev* **52**:71–81.

Petrova PS, Viller NN, Wong M, Pang X, Lin GH, Dodge K, Chai V, Chen H, Lee V, House V et al. (2017) TTI-621 (SIRPαFc): a CD47-blocking innate immune checkpoint inhibitor with broad antitumor activity and minimal erythrocyte binding. *Clin Cancer Res* **23**:1068–1079.

Qian BZ and Pollard JW (2010) Macrophage diversity enhances tumor progression and metastasis. *Cell* **141**:39–51.

Qiao C, Lv M, Li X, Geng J, Li Y, Zhang J, Lin Z, Feng J, and Shen B (2013) Affinity maturation of antiHER2 monoclonal antibody MIL5 using an epitope-specific synthetic phage library by computational design. *J Biomol Struct Dyn* **31**:511–521.

Ribas A, Hamid O, Daud A, Hodi FS, Wolchok JD, Kefford R, Joshua AM, Patnaik A, Hwu WJ, Weber JS et al. (2016) Association of pembrolizumab with tumor response and survival among patients with advanced melanoma. *JAMA* **315**:1600–1609.

Sharma P, Hu-Lieskovan S, Wargo JA, and Ribas A (2017) Primary, adaptive, and acquired resistance to cancer immunotherapy. *Cell* **168**:707–723.

Sikic BI, Lakhani N, Patnaik A, Shah SA, Chandana SR, Rasco D, Colevas AD, O'Rourke T, Narayanan S, Papadopoulos K et al. (2019) First-in-human, first-in-class phase I trial of the anti-CD47 antibody Hu5F9-G4 in patients with advanced cancers. *J Clin Oncol* **37**:946–953.

Starr JS, Jiang L, Li Z, Qiu Y, Menke DM, and Tun HW (2013) CD47 and osteopontin expression in diffuse large B-cell lymphoma with nodal and intravascular involvement. *Clin Lymphoma Myeloma Leuk* **13**:597–601.

Sudo T, Takahashi Y, Sawada G, Uchi R, Mimori K, and Akagi Y (2017) Significance of CD47 expression in gastric cancer. *Oncol Lett* **14**:801–809.

Veillette A and Chen J (2018) SIRPα-CD47 immune checkpoint blockade in anticancer therapy. *Trends Immunol* **39**:173–184.

Velliquette RW, Aeschlimann J, Kirkegaard J, Shakarian G, Lomas-Francis C, and Westhoff CM (2019) Monoclonal anti-CD47 interference in red cell and platelet testing. *Transfusion* **59**:730–737.

Wang Z, Wu Z, Liu Y, and Han W (2017) New development in CAR-T cell therapy. *J Hematol Oncol* **10**:53.

Weiskopf K, Jahchan NS, Schnorr PJ, Cristea S, Ring AM, Maute RL, Volkmer AK, Volkmer JP, Liu J, Lim JS et al. (2016) CD47-blocking immunotherapies stimulate macrophage-mediated destruction of small-cell lung cancer. *J Clin Invest* **126**:2610–2620.

Weiskopf K, Ring AM, Ho CC, Volkmer JP, Levin AM, Volkmer AK, Ozkan E, Fernhoff NB, van de Rijn M, Weissman IL et al. (2013) Engineered SIRPα variants as immunotherapeutic adjuvants to anticancer antibodies. *Science* **341**:88–91.

Xiao Z, Chung H, Banan B, Manning PT, Ott KC, Lin S, Capoccia BJ, Subramanian V, Hiebsch RR, Upadhya GA et al. (2015) Antibody mediated therapy targeting CD47 inhibits tumor progression of hepatocellular carcinoma. *Cancer Lett* **360**:302–309.

Zabuawala T, Taffany DA, Sharma SM, Merchant A, Adair B, Srinivasan R, Rosol TJ, Fernandez S, Huang K, Leone G et al. (2010) An ets2-driven transcriptional program in tumor-associated macrophages promotes tumor metastasis. *Cancer Res* **70**:1323–1333.

Address correspondence to: Longlong Luo, State Key Laboratory of Toxicology and Medical Countermeasures, Beijing Institute of Pharmacology and Toxicology, 27th Taiping Road, Beijing 100850, China. E-mail: luoll@bmi.ac.cn; or Hui Peng, School of Basic Medicine and Clinical Pharmacy, China Pharmaceutical University, Nanjing 210009, China & Department of Operational Medicine, Tianjin Institute of Environmental & Operational Medicine, Tianjin 300050, China. E-mail: p_h2002@hotmail.com

Figure S1

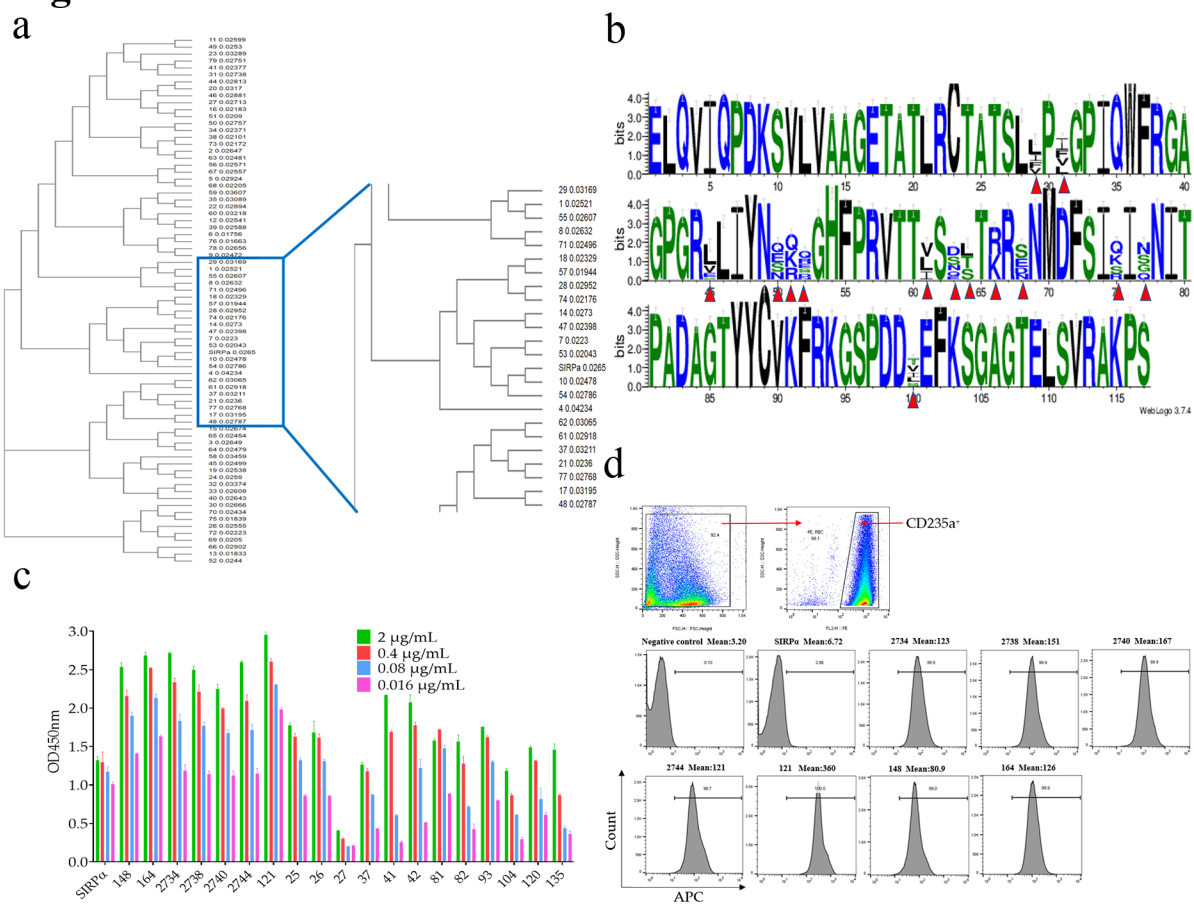

Figure S1. Library construction and selection. a. The library sequences were subjected to multiple sequence alignment using Clustal Omega. Sequences between each other have high homology in the phylogenetic tree, but there are some differences among them. **b**. The library sequences were analysed using Web Logo 3. All mutation sites in the correct sequence were theoretically designed mutation sites, the corresponding amino acids of the mutation sites were theoretically designed amino acids, and the frequency of each amino acid was equal. **c**. The activity of SIRPα mutant candidates binding to hCD47 was determined by ELISA. **d**. The activity of SIRPα mutant candidates binding to CD47 on the surface of RBCs was determined by FACS.

Figure S2

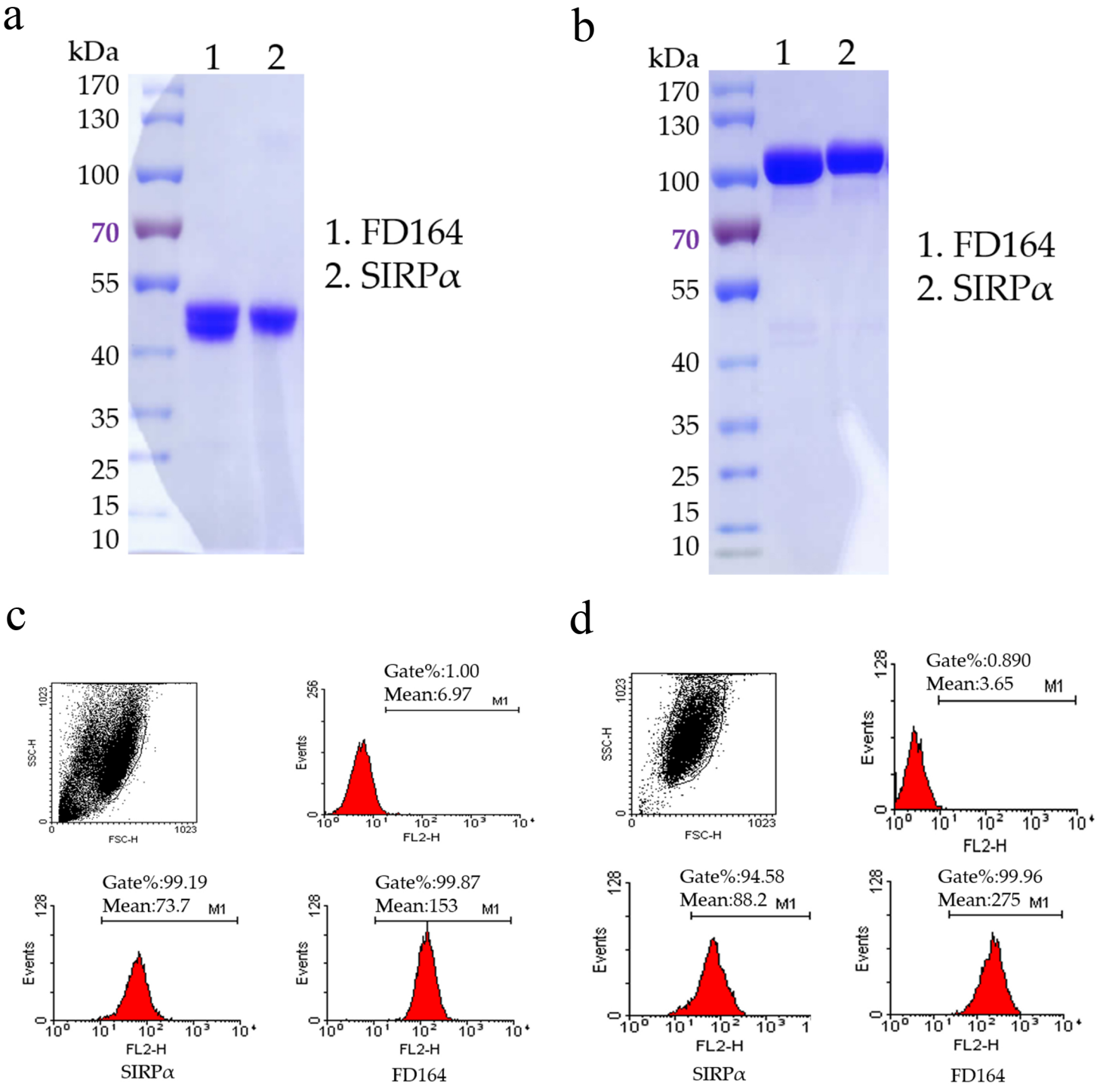

Figure S2. Analysis of purified proteins by agarose gel electrophoresis and the binding activity of FD164 to CD47 on the cancer cell lines by FACS. a. Reduced SDS-PAGE of purified proteins. **b**. Non-reduced SDS-PAGE of purified proteins. **c**. The binding activity of FD164 to CD47 on the Raji cells. **d**. The binding activity of FD164 to CD47 on the PC9 cells.